
This manuscript is a preprint and has not undergone peer-review. Please note that subsequent versions of this manuscript may have different content. If accepted, the final version of this manuscript will be available via the 'Peer-reviewed Publication DOI' link on the right-hand side of this webpage. Please feel free to contact any of the authors, we welcome feedback!

22 We combine high-resolution multibeam bathymetric and seismic reflection datasets
23 to investigate the reasons behind the significant changes in seabed morphology at the
24 scale of the Gippsland Basin. We reveal that in the northern region of the Gippsland
25 Basin, slope failures are the predominant sedimentary process, and giant submarine
26 landslides are therefore the major deposits in the northern region. Additionally, we
27 revealed that the submarine landslides are primed by the deposition and
28 accumulation of contourites generated by the East Australian Current. In the central
29 and southern regions, turbidity currents and canyoning processes are the major
30 sedimentary process. We indicate that the seasonal Bass Cascade Current can carry
31 large amounts of sediment, scour the seabed of the shelf and slope, and form turbidity
32 currents, canyons, and a series of other erosional seabed morphologies. We suggest
33 that slope gradient variation, different oceanography, and varied sedimentary
34 evolution processes have jointly contributed to seabed morphological complexity in
35 different regions of the Gippsland Basin. The high-resolution seabed morphological
36 analysis within this study provides critical geomorphological and geological
37 information for future submarine constructions (i.e. locating potential wind farms and
38 telecommunication cable installations) along with geohazard prediction and
39 mitigation (i.e. knowing the location of past and predicting future giant landslides).

40 Keywords: Gippsland Basin, Seabed morphology, Sedimentary processes, Submarine
41 landslides, Turbidity currents

42

43 INTRODUCTION

44 The Gippsland Basin is located on SE Australia's passive margin and it is one of
45 Australia's most prolific basins for hydrocarbon production, fishing, carbon storage,
46 and other marine resources (Figure 1A; Rahmanian et al., 1990; Mitchell et al., 2007a;
47 Mitchell et al., 2007b). Gippsland Basin hosts a variety of seabed morphologies, and
48 these seabed morphologies vary shiftily in different regions (Mitchell et al., 2007b).
49 From the shelf to the slope, seabed morphology is characterized by a number of
50 straight canyons, scarps, scours in channel templates, large linear canyons, channels,
51 gullies, and submarine landslides. The canyons and submarine landslides are initiated
52 from the continental shelf edge, are coalesced on the upper slope and captured by the
53 huge Bass Canyon at the lower slope, and ultimately drain SE to the Tasman Abyssal
54 Plain, where water depth ascends over 4000 m (Mitchell et al., 2007b). The complex
55 seabed morphology reflects the action of a range of oceanographic, sedimentological,
56 and tectonic processes at multiple spatiotemporal scales. However, the reasons why
57 the seabed morphology varies greatly from different regions and what controls the
58 complexity of seabed morphology are less well documented in the Gippsland Basin.
59 Therefore, this study aims to address the following questions: (i) what are the
60 dominant sedimentary processes in different regions of the Gippsland Basin? and (ii)
61 How is the morphology of the seabed changing rapidly in different regions of the
62 Gippsland Basin?

63

64 We combine bathymetric multibeam and seismic reflection datasets to understand the
65 form and evolution of seabed morphology, and to investigate the dominant

66 sedimentary processes in the Gippsland Basin. First, we aim to delineate the
67 morphological features in different regions of the Gippsland Basin, along the
68 continental shelf and slope areas. Second, we provide an interpretation of the
69 sedimentary processes that are active in shaping these morphological features. Finally,
70 we investigate the influence of oceanography and other factors on the development
71 of these sedimentary systems and explain how sedimentary processes are altered in
72 different regions of the Gippsland Basin. The results of this work could provide critical
73 geological information for future submarine construction (i.e., locating potential wind
74 farms and telecommunication cable installations) and geohazard prevention (i.e.
75 knowing the location of giant landslides) in the Gippsland Basin. Additionally, the
76 results of this study could serve as a valuable analogue to other similar submarine
77 settings globally.

78

79 GEOLOGICAL SETTING

80 *The Gippsland Basin*

81 The Gippsland Basin is Australia's easternmost continental margin basin, located
82 between the mainland of Australia and Tasmania (Figure 1A; Rahmanian et al., 1990).

83 The Gippsland Basin is approximately 400 km long and 80 km wide, with 80% of the
84 basin currently located offshore (Hocking, 1972; Willcox et al., 1992). The Gippsland
85 Basin belongs to a series of rift basins formed along the southern margin of the
86 Australian plate, due to the separation of the Antarctica and Australian continents
87 during the breakup of Gondwana in the Mesozoic (Colwell et al., 1993). The basin is

88 internally divided by four sets of approximately E-W oriented fault systems, including
89 the Rosedale and Lake Wellington Fault systems to the north, and the Foster and
90 Darriman Fault systems to the south (Figure 1C; Hegarty et al., 1985). These major fault
91 complexes separate the basin into several structural areas, including the Northern,
92 Central and Southern areas respectively (Figure 1C; Hegarty et al., 1985). The SE
93 margin of the Gippsland Basin is connected by c. 120 km long and 15-70 km wide, ESE-
94 trending Bass Canyon system (Figure 1C). The Bass Canyon has acted as a major
95 conduit and key element in the source-to-sink system in the SE Australian area since
96 the Late Cretaceous (approximately 80 Ma; Hill et al., 1998).

97

98 *Oceanography*

99 The Northern region of the Gippsland Basin is influenced by the Eastern Australian
100 Current (EAC; Mitchell et al., 2007b). The EAC meanders south along the east coast of
101 Australia, flowing at a velocity of c. 7.4 km/h (Suthers et al., 2011). The EAC carries
102 warm tropical seawater from the Coral Sea southwards to mix with the cool temperate
103 water of the Tasman Sea (Figures 1A, 1B). The EAC southwards heat transport has
104 increased the intensity and location of storms and wave actions (i.e. eddies), resulting
105 in complex topography along the eastern Australian coastline (Figure 1B; Ridgway and
106 Hill, 2009). The Southern and Central regions of the Gippsland Basin are influenced by
107 the seasonal Bass Cascade Current (BCC) (Figures 1A, 1C; Mitchell et al., 2007b). The
108 BCC belongs to a climate-driven, seasonal oceanographic phenomenon that is often
109 termed a dense shelf water cascade (Ivanov et al., 2004). The BCC was formed due to

110 the cold, denser Bass Strait seawater flowing into and sinking beneath the warmer,
111 fresher water of the Gippsland shelf, generating a northeast flowing current and
112 sinking to the 200-400 m isobath and extending tens of kilometres (Godfrey et al., 1980;
113 Li et al., 2005; Mitchell et al., 2007b). The BCC can travel at a high speed (with an
114 average transport rate of 3.6 km³/h) and is highly erosive (Godfrey et al., 1986). During
115 transportation, the BCC can affect a large portion of the seabed, create erosion and
116 carry significant amounts of sediments and spread along the shelf edge over a long
117 distance (Boland, 1971; Mitchell et al., 2007b). In Central regions, the BCC could
118 interact with seabed scarps (i.e. submarine landslide-generated scarps) and transform
119 into gravity flows (dominantly turbidity currents) that transport across the shelf, and
120 downslope over tens and hundreds of kilometres (Wu et al., 2023).

121

122 DATASET

123 Multibeam bathymetry data for this study is gridded at 50x50 m, and sourced from
124 Geoscience Australia's Marine data portal (<http://marine.ga.gov.au>). The multibeam
125 bathymetry dataset covers the Gippsland Basin continental shelf, at around 200 m
126 water depth, to the Tasman Sea Abyssal plain, at over 4000 m water depth (Figures
127 2A&2B). Two types of seismic reflection data are adopted in this study: (i) five 2D
128 regional seismic sections up to c. 1500 km long, therefore providing excellent coverage
129 from the Gippsland Basin shelf region to Bass Canyon abyssal plain (Figures 3A-D, 4B);
130 and (ii) three 3D seismic reflection surveys, including Elver 3D, Tuskfish 3D, and Oscar
131 3D (reprocessed in 2012), which cover an area of c. 650 km², 1050 km², and 1200 km²,

132 respectively (Table 1, Figure 2B). The 3D seismic datasets are zero-phase; with a SEG
133 normal polarity where a downward decrease and increase in acoustic impedance are
134 expressed as blue (negative) and red (positive) seismic reflections, respectively. We
135 calculate an approximate vertical resolution of c. 10-12.5 m for the near seabed
136 sediments, using the dominant frequency content of 40/50 hertz and an average
137 seismic velocity of 1700 m/s for the near seabed sediment.

138

139 RESULTS

140 Northern region

141 The Northern region spans 120 km long and 90 km wide (Figures 2B, 4A). In the
142 regional seismic sections, the continental shelf area has a gently dipping ($<1^\circ$) seabed
143 with an average water depth of 110–150 m (Figures 3A, 3B). Based on the slope
144 gradient, we subdivide the Northern region into the eastern and western parts (Figure
145 4A). In the eastern part, the shelf break marks a gradual transition from a shallow-
146 dipping (0.75°) shelf to a relatively steep (2.27°) slope, at approximately 1500 m water
147 depth (Figure 3A). In the western part, the shelf break marks a distinct transition from
148 the shallow-dipping shelf (0.08°) to a steep dipping slope (7.82°) at approximately 1000
149 m water depth (Figure 3B). In the following part, we describe the morphological
150 features and interpret their associated sedimentary processes from the continental
151 shelf to the slope area.

152

153 **Observation:** In the eastern part, extensively distributed giant scarps are observed

154 near the shelf edge and on the slope, where a single scarp can reach more than c. 30
155 km wide and nearly 400 m deep (Figures 4A, 4B). At least two submarine landslides
156 (landslide-1 and landslide-2) with scallop-shaped external geometry are observed on
157 the slope, occurring on the seabed gradient of c. 20° (Figure 4A). These landslides are
158 prodigious in scale, and the biggest landslide can extend for at least 25 km wide and
159 40 km long, involving an area of c. 700 km² (Landslide-1 in Figure 4A). Within these
160 landslides, a series of scallop-shaped internal scarps that form a terraced pattern are
161 observed (Figure 4A). In the seismic section, the scallop-shaped scarps are nested in a
162 stair-like style, showing a truncated reflector that cuts through upslope strata (see red
163 box in Figure 4B).

164

165 A shelf-indented canyon (Everard Canyon) that is initiated from the outer shelf is found
166 in the middle part of the Northern shelf (Figure 4A). The head of the Everard Canyon
167 is c. 40 km upslope to the shelf break, initiating at a water depth of 200 m and
168 extending to the lower slope where the water depth is more than 3500 m (Figure 4A).
169 The canyon head is characterised by a dendritic shape, comprising a major branch and
170 two deep landward excavated tributaries (Figure 4A). The upper section of Everard
171 Canyon initially dips SE, then alters its direction to NE-SW as it debouches to the edge
172 of the shelf (Figure 4A). On the shelf, terrace-shaped scarps are evident above the
173 eastern canyon sidewall but less pronounced above the western sidewall (Figure 4A).
174 In a cross-sectional view, Everard Canyon is characterised by U-shaped geometry, with
175 steep sidewalls of c. 30°, a width of c. 1.6 km and relief of c. 600 m (Figure 4B).

176 Additionally, no seismically visible deposition is observed on the canyon floor (Figure
177 4B). On the lower slope, Everard Canyon internally contains multiple scarps (Figure 4A).
178 In a dip-sectional profile cut along Everard Canyon, these multiple scarps are
179 characterised by a stair-shaped geometry with an upslope migration trend (Figure 4C).
180 Adjacent to Everard Canyon, three small-scale slope-confined canyons (Shark, Sole,
181 and Whaleshark Canyons) originate from the lower slope and intersect Bass Canyon at
182 their lower ends (Figure 4A). These slope-confined canyons dissipate above the lower
183 slope to a point canyon head and are characterised by a U-shaped cross-sectional
184 geometry (Figure 4D). The scale of these canyons ranges from 1.8-2.4 km in width and
185 c. 80 m-140 m in depth (Figure 4D). In the western part of the Northern region,
186 numerous slide scarps are evident on the continental shelf where the slope gradient is
187 $<1^\circ$ (Figure 5A). These scarps are spatially connected, making the morphology of the
188 outer shelf extremely complex. Generally, these scarps dip from east to west, with
189 widths ranging from c. 5 km to 20 km. In seismic sections, these slide scarps are nested
190 in a stair-shaped, backward (i.e. landward) dipping geometry, showing a truncated
191 reflector that cuts through upslope sediments (Figure 5B). Beneath the seabed, a
192 series of sub-parallel to wavy, alternating medium- to high-amplitude, internal
193 truncated seismic reflections with channel-shaped external forms are identified in the
194 seismic sections (Figures 5B, 5C). Parallel and continuous reflections with mounded
195 external forms are adjacent to the channel-shaped seismic packages (Figures 5B, 5C).
196
197 Further downslope to the slide scarps, widespread seabed gullies are oriented

198 perpendicular to the local slope contours and dip toward the south and southeast in
199 the slope area (Figure 4A). The gullies originated from the northern shelf edge and fed
200 into the eastern boundary of Bass Canyon. They are characterised by a set of straight,
201 closely spaced (130-280 m), sub-parallel and channel-shaped features. In cross-section,
202 gullies are V-shaped and steep-sided, with a relief (incision depth) of 40-170 m and a
203 width of 300-500 m (Figure 4E).

204

205 **Interpretation:** The presence of the stair-stepped scarps in the eastern part indicates
206 that the landslides are initiated at the lowermost part of the slope and propagated
207 retrogressively towards the upper slope (i.e. Sawyer et al., 2009; Wu et al., 2022). In
208 the western part, the scattered scarps on the shelf suggest that slope failures dominate
209 the continental shelf area. The water depth of the shelf is between 200-500 m, where
210 cyclic wave loading can constantly rework seabed sediments and account for the
211 potential trigger mechanism that results in slope failure (i.e. Marshall et al., 1978; Bea
212 et al., 1983). Further downslope, the dip direction of gullies is sub-perpendicular to
213 the strike direction of the scarps. This proximity of the scarps and gullies indicates the
214 latter originated from slope failures (i.e. Gardner et al., 1999; Gales et al., 2012). The
215 repetitive slope failures occurring on the shelf are likely to generate stable debris flows
216 and turbidity currents that are continuously transported downslope, which erode the
217 seabed and contributes to the initiation of gullies (i.e. Micallef and Mountjoy, 2011;
218 Lonergan et al., 2013).

219

220 On the shelf, the seismic expressions of channel-shaped seismic packages are similar
221 to those of buried contourite channels (Faugères et al., 1999; Stow et al., 2002), and
222 the mounded seismic packages are similar to buried contourite drifts (Figures 5B, 5C;
223 Miramontes et al., 2021). The deposition of the buried contourite channels and drifts
224 are attributed to the presence of the along-slope current, we infer that the along-slope
225 current flow towards the SW-WSW, as the current direction, is generally perpendicular
226 (Flood, 1988) or oblique (Blumsack and Weatherly, 1989) to contourite channel crests.
227 As the SW-flowing EAC is the major current that operates in the Northern region of the
228 Gippsland basin, we infer that the EAC is most probably responsible for the formation
229 of the buried contourite channels and drifts.

230

231 Everard Canyon is the largest tributary to Bass Canyon, it has not connected with any
232 fluvial system, meaning that there is limited terrestrial input from landward (Figure 2B;
233 Mitchell et al., 2007b). The alongshore movement of EAC has consistently transported
234 sediments into the head area of Everard Canyon (Mitchell et al., 2007b). Our
235 observations suggest that the SW propagating EAC would heavily impinge the eastern
236 canyon sidewall, causing slope failures and abundant scarps. The absence of
237 seismically visible intra-canyon infills suggests that the heads of Everard Canyon were
238 flushed by presently active erosional processes. We interpret that the most likely
239 erosional process is gravity flows generated by canyon sidewall failures (Wu et al.,
240 2022). The shift in the canyon transportation direction from SE to SW is primarily
241 controlled by the local topography created by the regional Rosedale Fault (Figure 1C).

242 The stair-shaped scarps developed within Everard Canyon near the lower slope
243 indicate long-term retrogressive failures that have occurred over time (Sawyer et al.,
244 2009). This may suggest that canyons in the Northern region are most likely to be
245 originated from the lower slope and migrate retrogressively through slope failure
246 processes (Farre et al., 1983; He et al., 2014).

247

248 Central Region

249 The continental shelf of the Central region extends seaward for approximately 70 km
250 at an average dip of 0.8° then abruptly steepens to an average dip of 8.8° reaching the
251 slope area (Figures 2B, 3C). The Central region has the steepest continental slope
252 within the study area. Our observations suggest this region is dictated by a different
253 oceanographic and sedimentary process relative to the Northern region.

254

255 **Observation:** On the shelf, multibeam and 3D seismic datasets document a c. 40 km-
256 long scarp that separates the undeformed shelf from a set of complex erosional
257 features (Figure 6A). Seismic sections cutting through the scarp reveal that well-
258 layered, undeformed strata are separated by moderately deformed, discontinuous
259 strata, bound by a high amplitude and continuous base surface (Figure 6B). East to the
260 scarp, a series of regularly spaced scour-shaped bedforms is observed near the SE part
261 of the shelf (Figure 6A). In the seismic section, the scour-shaped bedforms are
262 characterised by truncated, gently lee sides and short, steep stoss sides (Figure 6B).
263 Further north, scour-shaped bedforms are aligned in train and gradually form a

264 channel-shaped morphology (Figure 6A). In the seismic section, the scour-shaped
265 bedform train is also characterised by an erosional, steep lee side and a gently dipping
266 stoss side (Figure 6C). Further north of the shelf, at least two well-developed channels
267 are observed near the northern part of the shelf (Figure 6A). These channels initiate
268 from the outer shelf and extend to the shelf break (Figure 6A). They display trough-
269 shaped depressions with a flat base surface in the seismic cross-section (Figure 6D).
270 On the slope, widely distributed and predominant gullies extending from the shelf
271 edge to and intersecting with the Bass Canyon head are observed (Figure 6A). The
272 gullies are characterised by straight and linear morphology, dipping parallel to the
273 slope dip direction. The cross sections show the gullies are V-shaped, and have a clear
274 erosive truncation along the sidewalls (Figure 6E).

275

276 **Interpretation:** Wu et al. (2023) have thoroughly investigated the initiation and
277 evolution of these seabed morphologies and dominant sedimentary processes in the
278 Central region. It was suggested that the complex seabed morphology in this region is
279 genetically linked to a dynamic interaction between Bass Cascade Current, Westerly
280 wind, and strong waves (Wu et al., 2023). On the shelf, the NNE-trending scarp is
281 interpreted as the headwall scarp of a buried submarine landslide (Wu et al., 2023).
282 The scour-shaped bedforms and scour-shaped bedform train are interpreted as cyclic
283 steps and cyclic steps train, separately (i.e. Fildani et al., 2006). The presence of the
284 cyclic steps indicates turbidity currents are the dominant sedimentary process in the
285 Central region. Wu et al. (2023) suggest that the submarine landslides associated with

286 steep scarps can breach and subsequently catch the Bass Cascading Current, forcing
287 the current to transform into turbidity currents. After the turbidity currents initiation,
288 the steep scarps would then provide ample opportunity for the turbidity current to
289 evolve into Froude supercritical flow. The supercritical turbidity currents further
290 transport downslope, forming the widely distributed gullies and other erosional
291 structures on the slope. Additionally, Westerly winds generated waves, and storms
292 associated currents may also coincide with the Bass Cascading Current and jointly
293 resuspend seabed sediments and generate turbidity currents in the Central Gippsland
294 Basin (Wu et al., 2023). Thus, the transformed turbidity currents are an effective
295 seabed sculpting tool and hugely dictated the seabed morphology on the Central shelf
296 and slope.

297

298 Southern region

299 The Southern Region is c. 70 km long and c. 120 km wide (Figure 2B). In the regional
300 seismic section, the continental shelf area has a gently dipping (1.12°) seabed, and the
301 continental slope marks a gradual transition from a steep-dipping (5.37°) upper slope
302 to a gradual dipping (1.61°) lower slope, at approximately 3000 m water depth (Figure
303 3D).

304

305 **Observation:** In the Southern Region, the seabed is fairly featureless compared to the
306 Northern and Central regions, where gullies and mass failures are widely distributed
307 (Figure 7A). On the shelf, five shelf-indenting canyons extending from the continental

308 slope towards the downslope to converge with the Bass Canyon are observed (from
309 north to south: Anemone, Archer, Pisces, Moray and Mudskipper canyons; Figure 7A).
310 Canyons in the Southern region are evenly spaced (with intervals of c. 11-14 km),
311 flowing from E to SE, and oriented along the slope dip. On the upper slope, the canyons
312 display channel-like nature and show linear geometry with minor bifurcation (Figure
313 7A). On the middle slope, canyon geometry changes from linear to meander and then
314 shifts to bifurcate or even braid farther downslope, where the slope gradient is minor.
315 On the lower slope, canyons alter to sinuous stream-like features and gradually lose
316 expression and merge into the Bass Canyon (Figure 7A). In the upper part of these
317 canyons, the sidewalls of the canyon are typically steep, with occasional and localised
318 failures occurring along the headwalls and sidewalls (Figures 7B-C). Throughout the
319 course, canyons maintain a narrow, scour-deep, symmetric cross-sectional geometry
320 with a V-shaped profile (Figures 7B-7D).

321

322 On the shelf, several sets of scour-shaped bedforms that are aligned in a channel shape
323 have been imaged near the shelf breaks, adjacent to the canyon heads (Figure 8A). In
324 cross-section, the scour-shaped bedforms are morphologically asymmetric, with a
325 steep scarp on the lee side and a gentle dipping slope on the stoss side (Figure 8B).
326 The overall wavelength and height of these bedforms gradually decrease with water
327 depth (Figure 8C). Further downslope, straight and chute-like upper slope gullies
328 separated by distinct ridges are observed between Archer Canyon and Pisces Canyon
329 at a depth of 1000-1500 m (Figure 8A). These gullies have a limited distribution

330 compared to the gullies developed on the Northern and Central slopes. They are V-
331 shaped and steep-sided in cross-section, with a relief (incision depth) of 100-120 m
332 and a width of 800-1500 m (Figure 8C). Neither landslides nor scarps are evident
333 around or directly upslope the gullies (Figure 8A).

334

335 SE to the gullies, widely distributed scour-shaped bedforms with smaller scales are
336 observed in the upper-middle slope area (Figure 8A). A pattern of these bedforms can
337 be observed in the intra-canyon areas until the lower slope, where they remain
338 prominent (Figure 9A). Like their counterparts that developed on the shelf, they
339 feature steep lee sides and gentle stoss sides (Figures 8D, 9B). The scour-shaped
340 bedforms exhibit a distinct pattern of lateral transformation. More specifically, these
341 bedforms can convert into an incipient channel-shaped morphology, which eventually
342 evolves into a mature channel-shaped pattern (Figure 8A). On the middle slope, where
343 the slope gradient is less than 2° , extensive scarps are observed along the canyon
344 sidewalls (Figure 9A). These scarps have formed a block-shaped zone that is located
345 along the canyon sidewalls, showing a clear escarpment in the bathymetry cross-
346 section (Figure 9C).

347

348 **Interpretation:** On the shelf, the dendritic-shaped canyon heads indicate canyons are
349 in the juvenile stage of canyon development (Mitchell et al., 2007b). Canyon heads
350 entraining shelf sediments can constantly fuel erosive gravity flows that are
351 transported downslope along the canyon floor (Mitchell et al., 2007b). This explains

352 why canyons developed in the Southern region are featured with V-shaped canyon
353 profiles. Further downslope, the deflected canyon geometry is interpreted to be
354 caused by the path of canyons shifting over time, leaving the abandoned canyon
355 geometry near the middle- to lower- slope (Hill et al., 1998). Near the lower slope, the
356 block-shaped zone along the canyon sidewall is representative of erosional features
357 caused by repetitive canyon sidewall failures (i.e. Yin et al., 2019). Canyon sidewalls
358 can continue to steepen and destabilize, resulting in local failures and generating
359 turbidity currents, and steeping canyon sidewall gradients (Puga-Bernabéu et al.,
360 2013). We suggest that the continuation of this erosional process can provide local
361 sediment input to the canyon and maintain its propagation into the Bass Canyon, as
362 numerous channel-like features are identified on the Bass Canyon floor, suggesting
363 that Southern slope canyons are active, constantly transporting sediments into deep
364 marines (Figures 2A&2B).

365

366 The crescent-shaped bedforms are interpreted as cyclic steps that are usually caused
367 by turbidity currents during the excavation of the seabed through the force of
368 hydraulic jumps (Fildani et al., 2006; Zhong et al., 2015). The intimacy of the cyclic
369 steps developed on the shelf and the canyon heads indicates that turbidity currents
370 are active in modifying the canyon heads and providing sediment sources for the
371 canyon systems (Paull et al., 2002; Post et al., 2022). A continuous presence from cyclic
372 steps to gullies may indicate that the shelf and upper slope areas are continuously
373 shaped and remoulded by the turbidity current. The widespread distribution of cyclic

374 steps throughout the inter-canyon floor demonstrates the continuing role of turbidity
375 currents in shaping the seabed. The initiation of the turbidity currents is interpreted
376 as the volume of the intra-canyon downslope flowing currents being too large, and the
377 canyons cannot accommodate it, thus escaping the canyons and sweeping onto their
378 floors. Under the continuous erosion of the turbidity currents, the cyclic steps can
379 evolve into a cyclic step train, and the incipient channels, eventually forming the well-
380 developed channels (i.e. Fildani and Normark, 2004; Fildani et al., 2013).

381

382 DISCUSSION

383 *Northern region: East Australian Current and slope failure dominated*

384 On the Northern shelf, the thick accumulation of contourites may have played a role
385 in the preconditioning of the landslides (i.e. Brackenridge et al., 2020). The contourites
386 are generally fine-grained, poorly sorted, and have low permeabilities (Miramontes et
387 al., 2016; De Castro et al., 2020). Rapid deposition of such sediments favours the
388 generation of excess pore pressure and weak layers that can ultimately trigger slope
389 failures (Solheim et al., 2005; Gatter et al., 2020; Nicholson et al., 2020). In addition,
390 the deposition of contourite drifts can create a set of local high-gradient slopes that
391 can serve as slope failure susceptible structures, which increases slope instability and
392 lead to an increased likelihood of slope failures (Bryn et al., 2005; Rashid et al., 2017;
393 Miramontes et al., 2018).

394

395 The intense storms and wave actions created by the EAC along the Australian coastline

396 could also prime and trigger slope failures. Although the sedimentation rate is low
397 along the eastern Australian margin due to a combination of factors such as low
398 mainland sediment flux, limited accommodation space, and longshore drift is
399 generally assumed to have greater effect on sediment transport of the shelf sediments
400 (Short and Trenaman, 1992; Keene et al., 2008), recent studies showed that the EAC
401 has a more significant effect on upper and mid-slope margin sedimentation than
402 previously thought (Keene et al., 2008). In addition, the EAC flows southward as the
403 EAC Extension, along the east side of Bass Strait, reaching the east coast of Tasmania
404 (e.g., Ridgway and Dunn, 2003), and the eddies associated with the EAC are up to 200-
405 300 km in diameter, often 2-3 times annually, with a lifetime spanning more than a
406 year (Figure 1B; Boland and Church, 1981). These large-scale eddies follow a complex
407 southward trajectory and are generally constrained within slope settings (Boland and
408 Church, 1981; Ridgway and Hill, 2009). Therefore, eddies and cyclic wave loading can
409 continuously destabilise seabed sediments and ultimately trigger variously scaled
410 slope failures (i.e. Marshall et al., 1978; Bea et al., 1983). Additionally, historical
411 tsunamis have been identified along the Northern shelf since the Late Pleistocene
412 (Bryant and Price, 1997). Therefore, it is reasonable to presume that the Northern
413 region has a high hazard potential, representing a natural hazard region in the
414 Gippsland Basin. New geological and geophysical datasets (including sedimentary
415 cores, grabbing or dredging samples, additional high-resolution sub-bottom profiles,
416 3D seismic reflection data, crewed submersible dives, and Underwater Autonomous
417 Vehicles) are needed to assess modern seabed conditions (oceanographic and

418 geomorphology) and to provide better suggestions for future geohazard assessments.

419

420 *Southern and Central regions: Bass Cascade Currents and associated turbidity currents*

421 *dominate*

422 In the Southern region, the evenly spaced nature and the absence of onshore fluvial

423 systems indicate the canyoning process in the Southern region is fully marine and is

424 related to alongshore current activities (Krassay et al., 2004; Mitchell et al., 2007b; Wu

425 et al., 2022). Previous studies indicate the initiation and development of the canyons

426 are attributed to the strengthening of the Bass Cascade Current (BCC) since the

427 Pliocene (Mitchell et al., 2007a). Specifically, the BCC could carry a large amount of

428 suspended sediments and redeposit them on the southern shelf (Mitchell et al.,

429 2007b). This process could increase the sedimentation rate on the shelf and generate

430 downslope-eroding currents (Mitchell et al., 2007b). Observations of cyclic steps on

431 the shelf and slope suggest that the downslope-eroding currents are linked to

432 supercritical turbidity currents (i.e. Fildani et al., 2006; Zhong et al., 2015). Once the

433 turbidity currents are initiated, the canyon heads often play as the major conduits for

434 such currents (Canals et al., 2009; Morrison et al., 2020). Therefore, turbidity currents

435 are the dominant sedimentary processes in the Southern region.

436

437 The Central region also receives the seasonal arrival of the Bass Cascading Current

438 (BCC), along and across the continental shelf area (Mitchell et al., 2007b). The BCC can

439 work with pre-existing seabed scarps caused by submarine landslides and initiate

440 turbidity currents that travel from the shelf and reach the lower slope (Wu et.al 2023).
441 Compared to the Northern region, the influence of the EAC decreases significantly. A
442 major proportion of the EAC separates from the coast at the north of Sydney and
443 continues either towards New Zealand (Godfrey et al., 1980), leaving the EAC eddies
444 as one of the dominant oceanic inputs off northeast Tasmania during the summer
445 season (Cresswell and Legeckis, 1986). However, the eddies are generally constrained
446 within slope settings, and reach the maximum intensity between 30 and 35°S, and
447 therefore, do not have a strong influence on the Central and southern region of the
448 study area (Oke et al., 2019).

449

450 *What dictates the complexed seabed morphology in Gippsland Basin?*

451 The canyons developed in the Northern region are profoundly different from those
452 developed in the Southern region, in terms of their shape, scale and distribution (e.g.,
453 Figures 4A, 7A). More specifically, the canyons in the Northern region are generally
454 less incised (c. 50-100 m deep), and slope gradients are relatively flat (less than 10°).
455 In contrast, canyons developed in the Southern region often have more tributaries
456 with higher incision depths (more than 600 m) and steeper slope gradients (more than
457 35°). These differences might reflect different sedimentary processes, though the two
458 regions are only c. 40 km apart (Figures 2A, 4B).

459

460 In the Northern region, the slope-confined canyons (i.e. Sole and Shack canyons) are
461 located on the lower slope (Figure 4A). They are considered to evolve primarily

462 through local slope failures and progressively migrate upslope via retrogressive slope
463 failures (i.e. Farre et al., 1983; Jobe et al., 2011). The canyoning process originated
464 from slope failures initially occurring near the lower slope, further enlarged through
465 intra-canyon retrogressive failure and canyon sidewall collapses, extending upslope
466 direction and ultimately reaching the shelf edge (see the similar process from He et al.,
467 2014). Therefore, the primary mechanisms for canyon initiation and evolution are tied
468 to retrogressive slope failures, which start at the lower slope (i.e. Pratson and Coakley,
469 1996; He et al., 2014). In the Southern region, evidence for submarine landslides is
470 only present within the deeply incised dendritic canyon heads (i.e. Figure 7A).
471 Therefore, the slope failures might become important in the canyon development, but
472 they have limited contribution to the canyon initiation. On the Southern slope, the
473 presence of cyclic steps, cyclic step train and channels may represent a channel
474 evolution process (Figure 8A; i.e. Fildani and Normark, 2004; Fildani et al., 2013). The
475 cyclic steps represent morphodynamical signals of the incipient, early incision stage of
476 a channel (Fildani et al., 2013). With the repetitive flushing of the supercritical turbidity
477 currents, the cyclic scours and cyclic steps could develop into gullies or incipient
478 channels and ultimately evolve into canyons (as we observed from the upper slope;
479 8A). Therefore, in the Southern region, the primary mechanisms for canyon initiation
480 are linked to the downslope erosional process caused by turbidity currents (Fildani et
481 al., 2013).

482

483 Slope gradients could also influence seabed morphology. For example, the canyons are

484 linear in the Northern region, where the seafloor gradient is relatively high, and no
485 bifurcation nor diversion is observed (Figure 4A). While in the Southern region, when
486 canyons run into the low gradient lower slope ($\sim 1^\circ$), canyons initiate to meander and
487 bifurcate (Figure 9A). The lower slope gradient in the Southern region also explains
488 why gullies are intensively distributed on the Northern and Central slopes but are less
489 abundant on the Southern slope. This is because the threshold of slope gradient for
490 initiation of gullies is above 5.5° (Micallef and Mountjoy, 2011), while the Southern
491 slope only has an average slope gradient of 5.37° . We suggest that oceanography
492 directly influences sedimentary processes, thus controlling the morphology of the
493 seabed. For example, in the Central and Southern regions, the along-shelf transported
494 BCC has generated downslope flowing turbidity currents that have caused erosion in
495 the shelf and slope areas. Due to the presence of prevailing BCC, erosional features
496 related to morphology, such as channels, gullies, and canyons, dominate these areas.
497 In the Northern region, the prevalence of East Australian Current has created a slope
498 failure-prone environment, making widely distributed scarps and giant landslides the
499 major morphology.

500

501 CONCLUSION

502 We combine high-resolution bathymetrical, and 2D and 3D seismic reflection datasets
503 to investigate the seabed morphology and sedimentary processes in the Gippsland
504 Basin, SE Australia. Our results show that the seabed morphology varies significantly
505 between different regions of the Gippsland Basin. We reveal that in the Northern

506 Region, the East Australian Current could prime slope failures and cause dominant
507 landslide morphologies. In the Central and Southern regions, the Bass Cascade Current
508 could initiate turbidity currents that cause a series of erosional morphologies. We
509 indicate that oceanography, sedimentary evolution processes, seabed gradients, and
510 tectonics have jointly contributed to the complexity of the seabed morphology in the
511 Gippsland Basin. The results of our study could provide new insights into process
512 interactions that influence seabed sedimentation and morphology, which are
513 particularly pertinent to submarine constructions and geohazard mitigations and can
514 be used for paleo-reconstruction interpretations.

515

516 **ACKNOWLEDGMENTS**

517 A grant from the Fundamental Research Funds of the Central Universities of China was
518 provided to conduct this research. The first author thanks the Shanghai Committee of
519 Science and Technology (under Grant No. 23ZR1467800) and the State Key Laboratory
520 of Marine Geology (under Grant No. MGZ202303) for their financial support. We thank
521 Geoscience Australia for providing valuable seismic and multibeam bathymetry for the
522 Gippsland Basin. We also thank Prof. Guangfa Zhong and Wei Li, Dr. Chao Liang for
523 their supportive suggestions that enrich this work.

524 **FIGURE CAPTIONS**

525 Figure 1. (A) Regional map of Australia, showing the location of the study area and the
526 oceanographic setting. BCC, Bass Cascade Current; EAC, East Australian Current. The
527 dashed yellow polygon indicates the location of Figure 1B, the solid black polygon
528 indicates the location of Figure 1C. (B) Seawater temperature map monitored on 14th
529 January, 2020, highlighting the speed and pathway of the EAC and the locations of its
530 associated eddies. Figure 1B is modified from the Integrated Marine Observing System
531 (IMOS) of Australia (<http://oceancurrent.imos.org.au/index.php>). (C) Zoom in view of
532 the Gippsland Basin and the Bass Canyon. The pathway of the BCC is adopted from
533 Tomczak (1985) and Tomczak (1987). The pathway of the EAC is adopted from Lavering
534 (1994) and Ridgway and Hill (2009). The regional faults were modified after Hill et al.
535 (1998) and O'Brien et al. (2018).

536

537 Figure 2. (A) Overview of hill-shaded seabed bathymetry map with contours (white
538 dotted line) depicting the main morphologic features in the study area and the north-
539 arrow (white). (B) Seabed slope gradient map with interpretations, showing the key
540 depositional elements, major canyon names, and location of 3D seismic datasets.

541

542 Figure 3. (A) Shelf to Slope profile showing the upper-, middle- and lower part of the
543 Northern slope. (B) Shelf to Slope profile depicting the upper-, middle- and lower part
544 of the western Northern region. (C) Shelf-to-slope profile traversing across the Central
545 shelf and slope regions. (D) Shelf to Slope profile illustrating the upper-, middle- and

546 lower part of the Southern region. See Figure 2B for locations.

547

548 Figure 4. (A) Multibeam bathymetric map (in slope gradient) in the Northern region.

549 (B) Seismic section across the Northern slope. (C) Bathymetric profile cut across the

550 gullies developed on the Northern slope. (D) Bathymetric profile extracted from the

551 long axis of Everard Canyon. (E) Cross-sectional bathymetric profile cutting across the

552 canyons in the lower slope area of the Northern region. See Figure 4A for locations.

553

554 Figure 5. (A) Seabed structure map of the Northern shelf calculated from 3D seismic

555 data. (B) Seismic dip section cutting along the scarps developed on the shelf. (C)

556 Seismic dip section cutting along the scarps developed on the shelf. See Figure 5A for

557 locations.

558

559 Figure 6. (A) Seabed bathymetric map calculated from 3D seismic data, showing the

560 seabed morphology in the Central region. (B) Seismic section cutting along the

561 headwall scarp and cyclic scours developed on the shelf. (C) Seismic section cutting

562 along the headwall scarp and cyclic step train developed on the shelf. (D) Seismic

563 section cutting across the cyclic step train and channels developed on the shelf. (E)

564 Seismic section cutting across the gullies that developed on the slope. See the location

565 in Figure 6A.

566

567 Figure 7. (A) Multibeam bathymetric map (in slope gradient) showing the

568 interpretations of the seabed morphologies in the Southern region. (B) Bathymetric
 569 profile cutting across the upper section of the canyons in the Southern shelf. (C)
 570 Bathymetric profile cutting across the middle section of the canyons in the Southern
 571 slope. (D) Bathymetric profile cutting across the lower section of the canyons in the
 572 Southern slope. See Figure 7A for locations.

573

574 Figure 8. (A) Multibeam bathymetric map (in slope gradient) shows the zoomed-in
 575 profile of the Southern shelf with interpretations of the seabed morphologies. See
 576 Figure 7A for location. (B) Along-slope bathymetric profile cut through cyclic steps
 577 developed on the shelf. (C) Bathymetric profile cut across the gullies and Pisces Canyon,
 578 showing their cross-sectional profiles. (D) Bathymetric profile cut along cyclic steps
 579 developed on the upper slope. See the location in Figure 8A.

580

581 Figure 9. (A) Multibeam bathymetric map (in slope gradient) shows the zoomed-in
 582 profile of the lower slope with interpretations of the seabed morphologies. See Figure
 583 7A for location. (B) Bathymetric profile cut along cyclic steps developed on the lower
 584 slope. (C) Bathymetric profile cut across the canyon on the lower slope. See the
 585 location in Figure 9A.

586

587 Table 1. 3D seismic reflection data and their properties used in the study.

Seismic data	Vintage	Water Depth (m)	Area (km ²)	Bin Size (m)		Frequency (Seabed)	Vertical Resolution (m)
				Xline	Inline		
Elver 3D	2007	150-2700	650	25	25	40	12.5
Tuskfish 3D	2004	150-2700	1050	12.5	18.75	50	10
Oscar 3D	2006	800-1500	1200	25	18.75	40	12.5

588

REFERENCE

- Boland, F., 1971, Temperature-salinity anomalies at depths between 200m and 800m in the Tasman sea: *Marine and Freshwater Research*, v. 22, no. 2, p. 55-62.
- Hocking, J. B., 1972, Geologic evolution and hydrocarbon habitat Gippsland Basin: *The APPEA Journal*, v. 12, no. 1, p. 132-137.
- Marshall, N., Stanley, D., and Kelling, G., 1978, Large storm-induced sediment slump reopens an unknown Scripps submarine canyon tributary: Sedimentation in submarine canyons, fans, and trenches: Stroudsburg, Pennsylvania, Hutchinson and Ross, p. 73-84.
- Godfrey, J., Jones, I., Maxwell, G., and Scott, B., 1980, On the winter cascade from Bass Strait into the Tasman Sea: *Marine and Freshwater Research*, v. 31, no. 3, p. 275-286.
- Boland, F., and Church, J., 1981, The east Australian current 1978: *Deep Sea Research Part A. Oceanographic Research Papers*, v. 28, no. 9, p. 937-957.
- Bea, R. G., Wright, S. G., Sircar, P., and Niedoroda, A. W., 1983, Wave-induced slides in south pass block 70, Mississippi Delta: *Journal of Geotechnical Engineering*, v. 109, no. 4, p. 619-644.
- Farre, J. A., McGregor, B. A., Ryan, W. B., and Robb, J. M., 1983, Breaching the shelfbreak: passage from youthful to mature phase in submarine canyon evolution.
- Hegarty, K., Duddy, I., Green, P., Gleadow, A., Fraser, I., and Weissel, J., 1985, Regional evaluation of the tectonic and thermal history of the Gippsland Basin.
- Tomczak, 1985, The Bass Strait water cascade during winter 1981: *Continental Shelf Research*, v. 4, no. 3, p. 255-278.
- Cresswell, G., and Legeckis, R., 1986, Eddies off southeastern Australia: *Deep Sea Research Part A. Oceanographic Research Papers*, v. 33, no. 11-12, p. 1527-1562.
- Godfrey, J., Vaudrey, D., and Hahn, S., 1986, Observations of the shelf-edge current south of Australia, winter 1982: *Journal of Physical Oceanography*, v. 16, no. 4, p. 668-679.
- Tomczak, M., 1987, The Bass Strait water cascade during summer 1981-1982: *Continental Shelf Research*, v. 7, no. 6, p. 561-572.
- Flood, R. D., 1988, A lee wave model for deep-sea mudwave activity: *Deep Sea Research Part A. Oceanographic Research Papers*, v. 35, no. 6, p. 973-983.
- Blumsack, S., and Weatherly, G., 1989, Observations of the nearby flow and a model for the growth of mudwaves: *Deep Sea Research Part A. Oceanographic Research Papers*, v. 36, no. 9, p. 1327-1339.
- Rahmanian, V., Moore, P., Mudge, W., and Spring, D., 1990, Sequence stratigraphy and the habitat of hydrocarbons, Gippsland Basin, Australia: Geological Society, London, Special Publications, v. 50, no. 1, p. 525-544.
- Short, A. D., and Trenaman, N., 1992, Wave climate of the Sydney region, an energetic and highly variable ocean wave regime: *Marine and Freshwater Research*, v. 43, no. 4, p. 765-791.
- Willcox, J., Colwell, J., and Constantine, A., 1992, New ideas on Gippsland Basin regional tectonics.
- Colwell, J. B., Constantine, A. E., and Willcox, J. B., 1993, Regional structure of the Gippsland Basin: interpretation and mapping of a deep seismic data set, Australian Geological Survey Organisation.
- Lavering, I. H., 1994, Marine environments of Southeast Australia (Gippsland Shelf and Bass Strait) and the impact of offshore petroleum exploration and production activity: *Marine georesources & geotechnology*, v. 12, no. 3, p. 201-226.
- Pratson, L. F., and Coakley, B. J., 1996, A model for the headward erosion of submarine canyons induced by downslope-eroding sediment flows: *Geological Society of America Bulletin*,

- v. 108, no. 2, p. 225-234.
- Bryant, E. A., and Price, D., 1997, Late Pleistocene marine chronology of the Gippsland Lakes region, Australia: *Physical Geography*, v. 18, no. 4, p. 318-334.
- Hill, P., Exon, N., Keene, J., and Smith, S., 1998, The continental margin off east Tasmania and Gippsland: structure and development using new multibeam sonar data: *Exploration Geophysics*, v. 29, no. 4, p. 410-419.
- Faugères, J.-C., Stow, D. A., Imbert, P., and Viana, A., 1999, Seismic features diagnostic of contourite drifts: *Marine Geology*, v. 162, no. 1, p. 1-38.
- Gardner, J. V., Prior, D. B., and Field, M. E., 1999, Humboldt slide—a large shear-dominated retrogressive slope failure: *Marine Geology*, v. 154, no. 1-4, p. 323-338.
- Paull, C., Ussler, W., Greene, H., Keaten, R., Mitts, P., and Barry, J., 2002, Caught in the act: the 20 December 2001 gravity flow event in Monterey Canyon: *Geo-Marine Letters*, v. 22, no. 4, p. 227-232.
- Stow, D. A., Faugères, J.-C., Howe, J. A., Pudsey, C. J., and Viana, A. R., 2002, Bottom currents, contourites and deep-sea sediment drifts: current state-of-the-art: *Geological Society, London, Memoirs*, v. 22, no. 1, p. 7-20.
- Ridgway, K., and Dunn, J., 2003, Mesoscale structure of the mean East Australian Current System and its relationship with topography: *Progress in oceanography*, v. 56, no. 2, p. 189-222.
- Fildani, A., and Normark, W. R., 2004, Late Quaternary evolution of channel and lobe complexes of Monterey Fan: *Marine Geology*, v. 206, no. 1-4, p. 199-223.
- Ivanov, V., Shapiro, G., Huthnance, J., Aleynik, D., and Golovin, P., 2004, Cascades of dense water around the world ocean: *Progress in oceanography*, v. 60, no. 1, p. 47-98.
- Krassay, A., Cathro, D., and Ryan, D., 2004, A regional tectonostratigraphic framework for the Otway Basin.
- Bryn, P., Berg, K., Forsberg, C. F., Solheim, A., and Kvalstad, T. J., 2005, Explaining the Storegga slide: *Marine and Petroleum Geology*, v. 22, no. 1, p. 11-19.
- Li, F., Dyt, C., Griffiths, C., Jenkins, C., Rutherford, M., and Chittleborough, J., 2005, Seabed sediment transport and offshore pipeline risks in the Australian southeast: *The APPEA Journal*, v. 45, no. 1, p. 523-534.
- Solheim, A., Berg, K., Forsberg, C., and Bryn, P., 2005, The Storegga Slide complex: repetitive large scale sliding with similar cause and development: *Marine and Petroleum Geology*, v. 22, no. 1-2, p. 97-107.
- Fildani, A., Normark, W. R., Kostic, S., and Parker, G., 2006, Channel formation by flow stripping: Large-scale scour features along the Monterey East Channel and their relation to sediment waves: *Sedimentology*, v. 53, no. 6, p. 1265-1287.
- Mitchell, J., Holdgate, G., and Wallace, M., 2007a, Pliocene–Pleistocene history of the Gippsland Basin outer shelf and canyon heads, southeast Australia: *Australian Journal of Earth Sciences*, v. 54, no. 1, p. 49-64.
- Mitchell, J., Holdgate, G., Wallace, M., and Gallagher, S., 2007b, Marine geology of the Quaternary Bass Canyon system, southeast Australia: a cool-water carbonate system: *Marine geology*, v. 237, no. 1-2, p. 71-96.
- Keene, J., Baker, C., Tran, M., and Potter, A., 2008, Sedimentology and Geomorphology of the East Marine region of Australia: *Geoscience Australia, Record*, v. 10.
- Canals, M., Danovaro, R., Heussner, S., Lykousis, V., Puig, P., Trincardi, F., Calafat, A. M., de Madron, X. D., Palanques, A., and Sanchez-Vidal, A., 2009, Cascades in Mediterranean submarine grand canyons: *Oceanography*, v. 22, no. 1, p. 26-43.
- Ridgway, K., and Hill, K., 2009, The East Australian Current.
- Sawyer, D. E., Flemings, P. B., Dugan, B., and Germaine, J. T., 2009, Retrogressive failures recorded in mass transport deposits in the Ursa Basin, Northern Gulf of Mexico: *Journal of Geophysical Research: Solid Earth*, v. 114, no. B10.

- Jobe, Z. R., Lowe, D. R., and Uchytíl, S. J., 2011, Two fundamentally different types of submarine canyons along the continental margin of Equatorial Guinea: *Marine and Petroleum Geology*, v. 28, no. 3, p. 843-860.
- Micallef, A., and Mountjoy, J. J., 2011, A topographic signature of a hydrodynamic origin for submarine gullies: *Geology*, v. 39, no. 2, p. 115-118.
- Suthers, I. M., Young, J. W., Baird, M. E., Roughan, M., Everett, J. D., Brassington, G. B., Byrne, M., Condie, S. A., Hartog, J. R., and Hassler, C. S., 2011, The strengthening East Australian Current, its eddies and biological effects—an introduction and overview, Volume 58, Elsevier, p. 538-546.
- Gales, J., Larter, R., Mitchell, N., Hillenbrand, C. D., Østerhus, S., and Shoosmith, D., 2012, Southern Weddell Sea shelf edge geomorphology: Implications for gully formation by the overflow of high-salinity water: *Journal of Geophysical Research: Earth Surface*, v. 117, no. F4.
- Fildani, A., Hubbard, S. M., Covault, J. A., Maier, K. L., Romans, B. W., Traer, M., and Rowland, J. C., 2013, Erosion at inception of deep-sea channels: *Marine and Petroleum Geology*, v. 41, p. 48-61.
- Lonergan, L., Jamin, N. H., Jackson, C. A.-L., and Johnson, H. D., 2013, U-shaped slope gully systems and sediment waves on the passive margin of Gabon (West Africa): *Marine Geology*, v. 337, p. 80-97.
- Puga-Bernabéu, Á., Webster, J. M., Beaman, R. J., and Guilbaud, V., 2013, Variation in canyon morphology on the Great Barrier Reef margin, north-eastern Australia: The influence of slope and barrier reefs: *Geomorphology*, v. 191, p. 35-50.
- He, Y., Zhong, G., Wang, L., and Kuang, Z., 2014, Characteristics and occurrence of submarine canyon-associated landslides in the middle of the northern continental slope, South China Sea: *Marine and Petroleum Geology*, v. 57, p. 546-560.
- Zhong, G., Cartigny, M. J., Kuang, Z., and Wang, L., 2015, Cyclic steps along the South Taiwan Shoal and West Penghu submarine canyons on the northeastern continental slope of the South China Sea: *Bulletin*, v. 127, no. 5-6, p. 804-824.
- Miramontes, E., Cattaneo, A., Jouet, G., Thereau, E., Thomas, Y., Rovere, M., Cauquil, E., and Trincardi, F., 2016, The Pianosa contourite depositional system (northern Tyrrhenian Sea): Drift morphology and Plio-Quaternary stratigraphic evolution: *Marine Geology*, v. 378, p. 20-42.
- Rashid, H., MacKillop, K., Sherwin, J., Piper, D., Marche, B., and Vermooten, M., 2017, Slope instability on a shallow contourite-dominated continental margin, southeastern Grand Banks, eastern Canada: *Marine Geology*, v. 393, p. 203-215.
- Miramontes, E., Garziglia, S., Sultan, N., Jouet, G., and Cattaneo, A., 2018, Morphological control of slope instability in contourites: a geotechnical approach: *Landslides*, v. 15, no. 6, p. 1085-1095.
- O'Brien, P., Mitchell, C., Nguyen, D., and Langford, R., 2018, Mass Transport Complexes on a Cenozoic paleo-shelf edge, Gippsland basin, southeastern Australia: *Marine and Petroleum Geology*, v. 98, p. 783-801.
- Oke, P. R., Roughan, M., Cetina-Heredia, P., Pilo, G. S., Ridgway, K. R., Rykova, T., Archer, M. R., Coleman, R. C., Kerry, C. G., and Rocha, C., 2019, Revisiting the circulation of the East Australian Current: Its path, separation, and eddy field: *Progress in Oceanography*, v. 176, p. 102139.
- Yin, S., Lin, L., Pope, E. L., Li, J., Ding, W., Wu, Z., Ding, W., Gao, J., and Zhao, D., 2019, Continental slope-confined canyons in the Pearl River Mouth Basin in the South China Sea dominated by erosion, 2004–2018: *Geomorphology*, v. 344, p. 60-74.
- Brackenridge, R. E., Nicholson, U., Sapiie, B., Stow, D., and Tappin, D. R., 2020, Indonesian Throughflow as a preconditioning mechanism for submarine landslides in the Makassar Strait: *Geological Society, London, Special Publications*, v. 500, no. 1, p. 195-

- De Castro, S., Hernández-Molina, F., Rodríguez-Tovar, F., Llave, E., Ng, Z., Nishida, N., and Mena, A., 2020, Contourites and bottom current reworked sands: Bed facies model and implications: *Marine Geology*, v. 428, p. 106267.
- Gatter, R., Clare, M. A., Hunt, J. E., Watts, M., Madhusudhan, B., Talling, P. J., and Huhn, K., 2020, A multi-disciplinary investigation of the AFEN Slide: the relationship between contourites and submarine landslides: *Geological Society, London, Special Publications*, v. 500, no. 1, p. 173-193.
- Morrison, A., Hogg, A. M., England, M. H., and Spence, P., 2020, Warm Circumpolar Deep Water transport toward Antarctica driven by local dense water export in canyons: *Science advances*, v. 6, no. 18, p. eaav2516.
- Nicholson, U., Libby, S., Tappin, D. R., and McCarthy, D., 2020, The Subantarctic Front as a sedimentary conveyor belt for tsunamigenic submarine landslides: *Marine Geology*, v. 424, p. 106161.
- Miramontes, E., Thiéblemont, A., Babonneau, N., Penven, P., Raison, F., Droz, L., Jorry, S. J., Fierens, R., Counts, J. W., and Wilckens, H., 2021, Contourite and mixed turbidite-contourite systems in the Mozambique Channel (SW Indian Ocean): Link between geometry, sediment characteristics and modelled bottom currents: *Marine Geology*, v. 437, p. 106502.
- Post, A. L., Przeslawski, R., Nanson, R., Siwabessy, J., Smith, D., Kirkendale, L. A., and Wilson, N. G., 2022, Modern dynamics, morphology and habitats of slope-confined canyons on the northwest Australian margin: *Marine Geology*, v. 443, p. 106694.
- Wu, N., Nugraha, H. D., Zhong, G., and Steventon, M. J., 2022, The role of mass-transport complexes in the initiation and evolution of submarine canyons: *Sedimentology*.
- Wu, N., Zhong, F. G., Niyazi, Y., Nugraha, H. D., and Steventon, M., 2023, Transformation of dense shelf water cascade to supercritical turbidity currents: Impact on seabed geomorphology and implication for climate change.

Figure 1

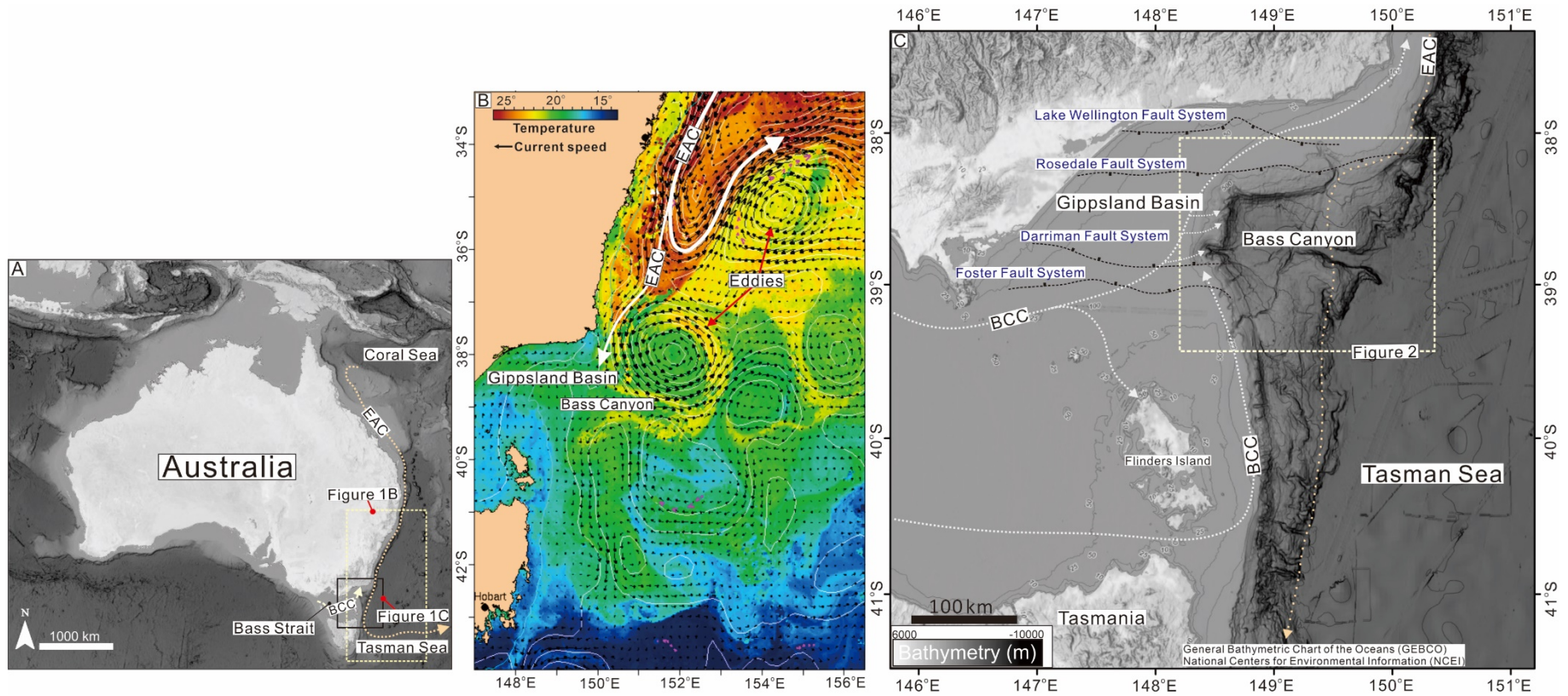


Figure 2

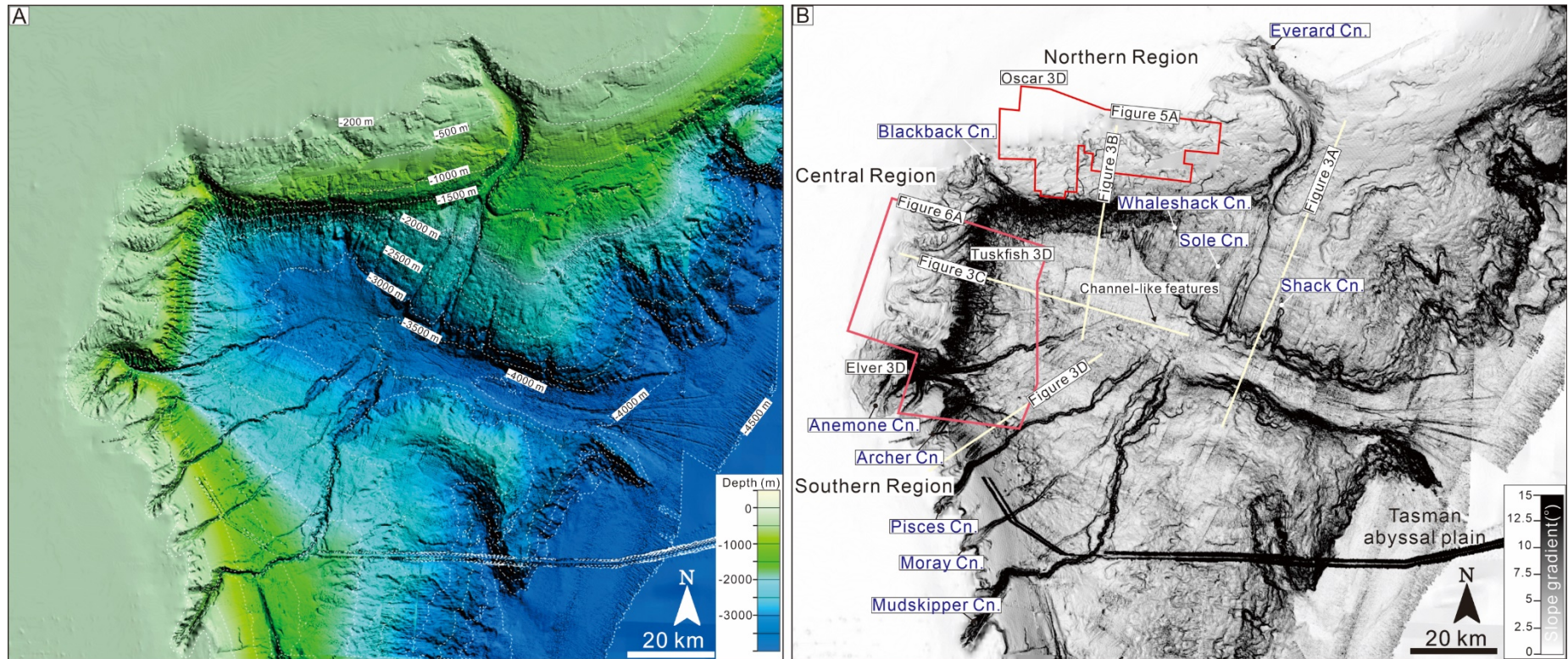


Figure 3

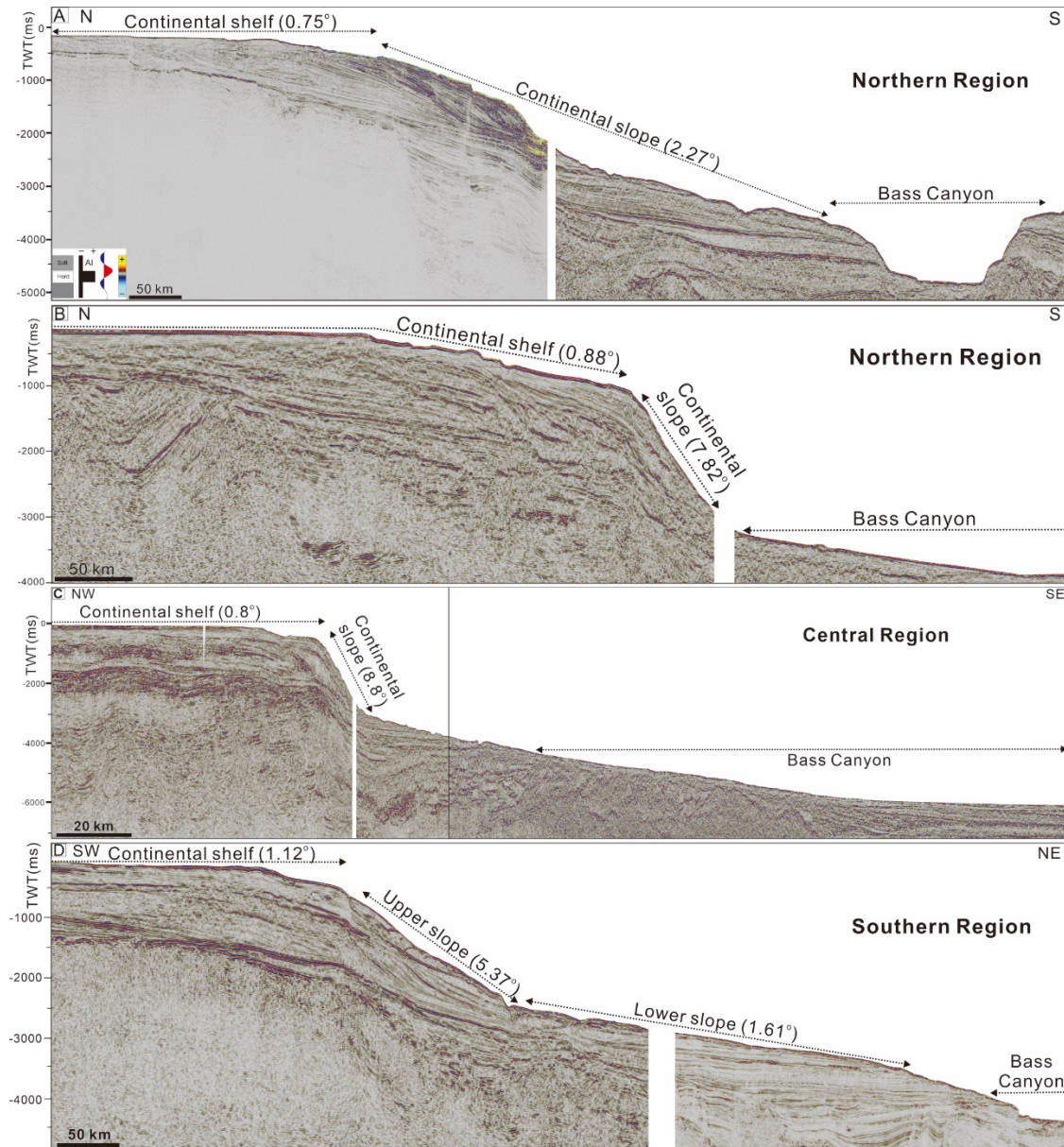


Figure 4

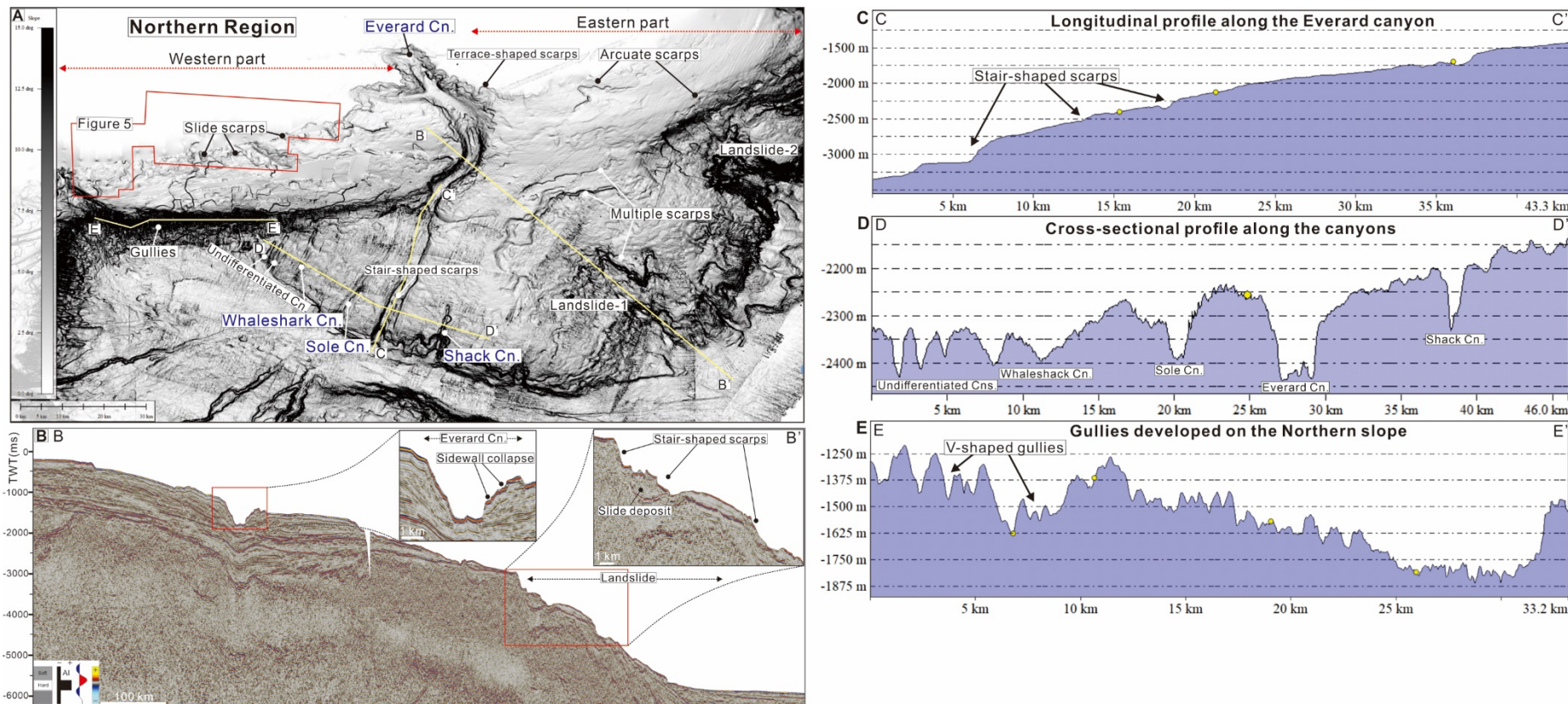


Figure 5

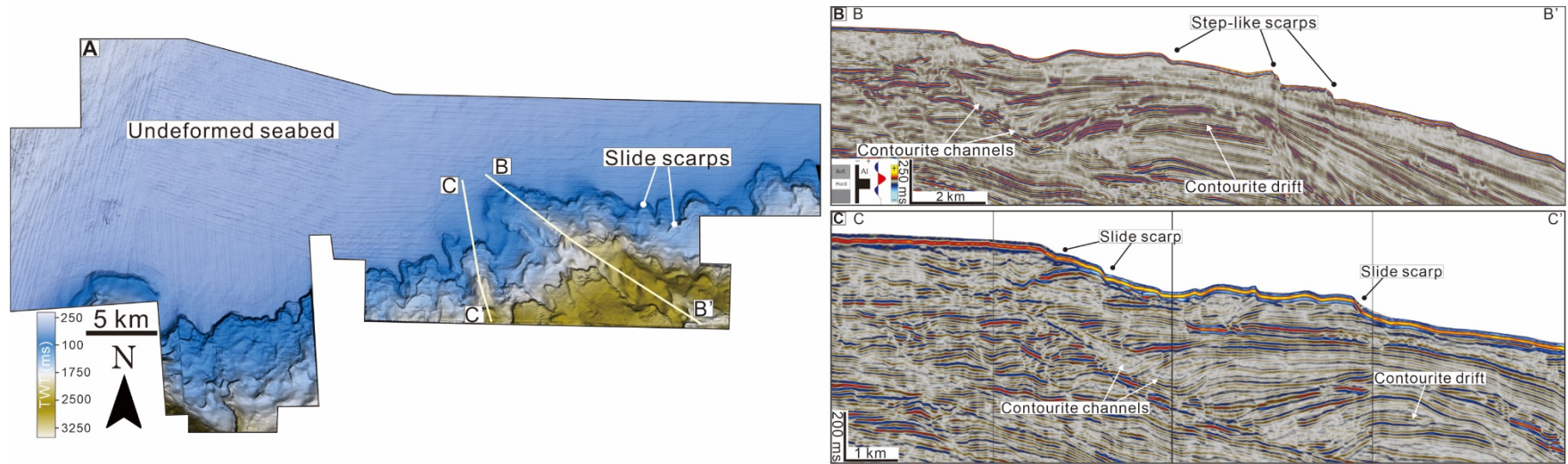


Figure 6

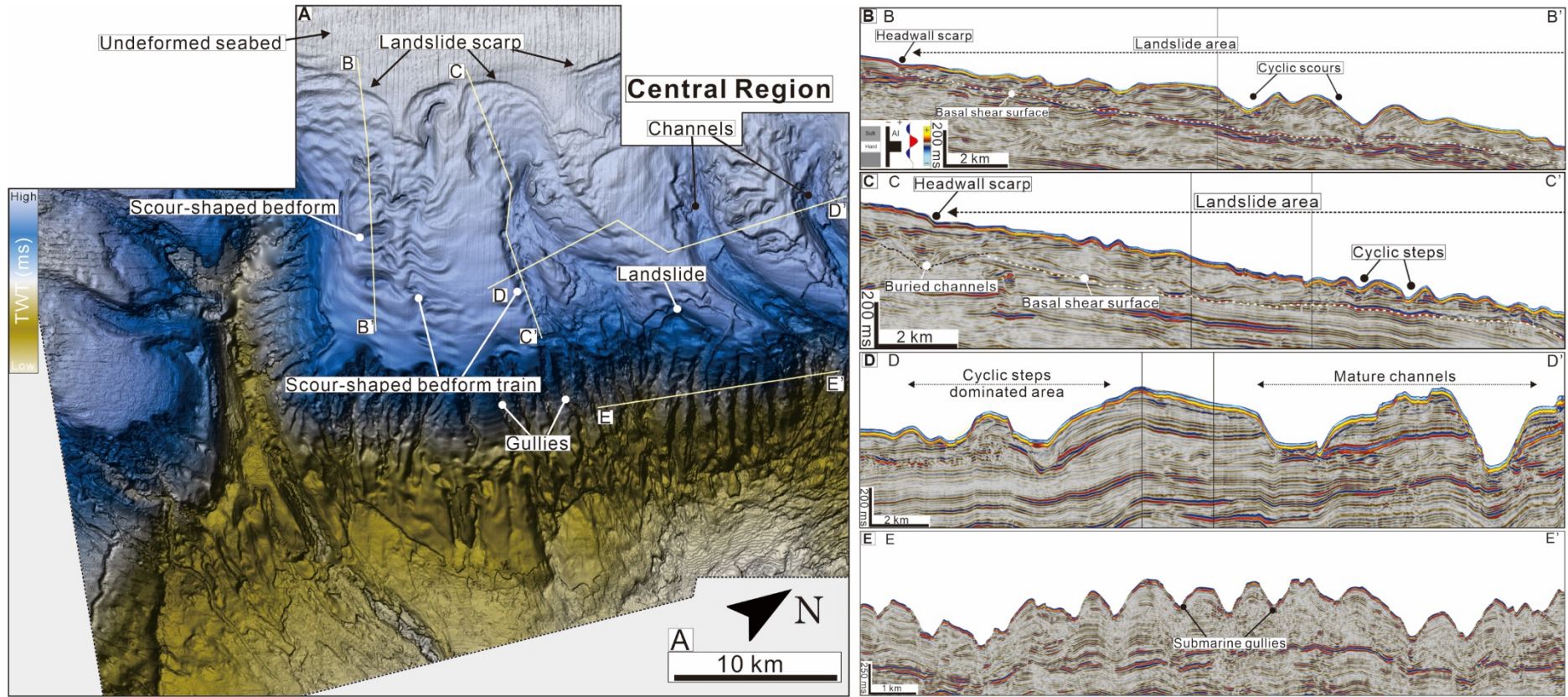


Figure 7

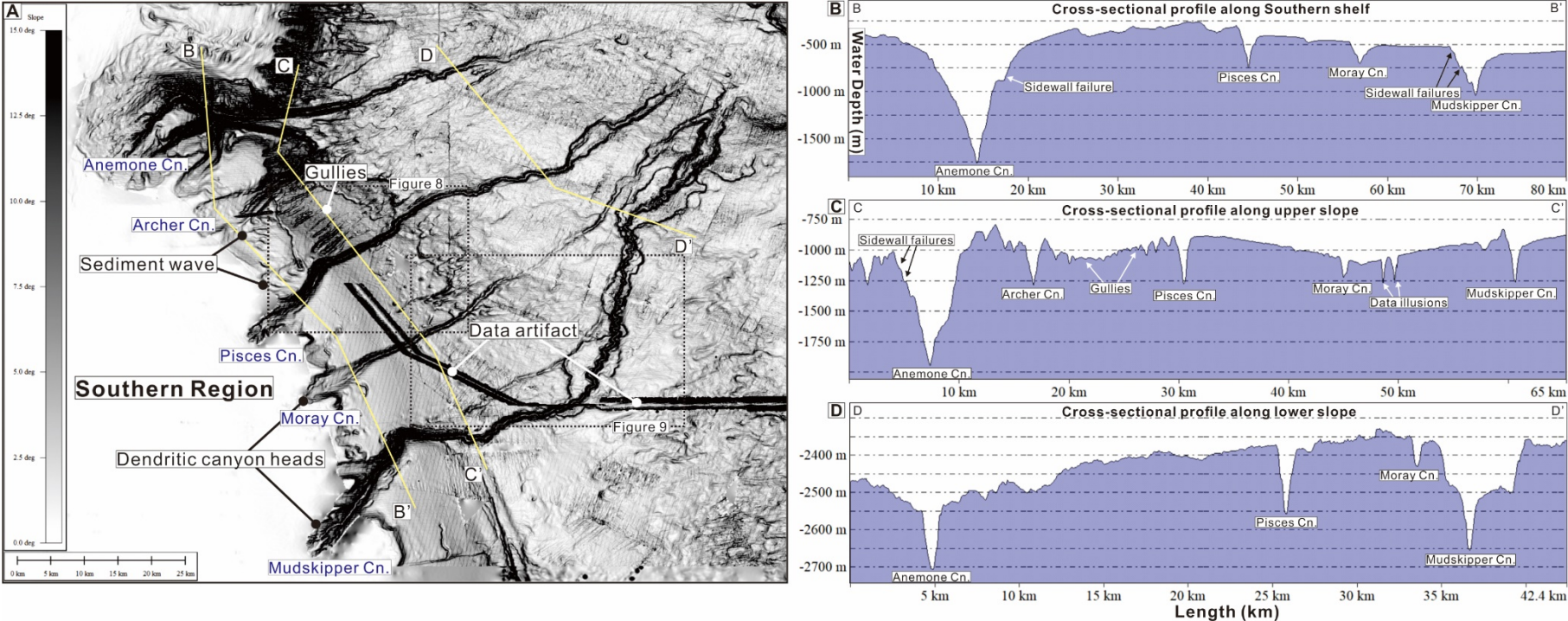


Figure 8

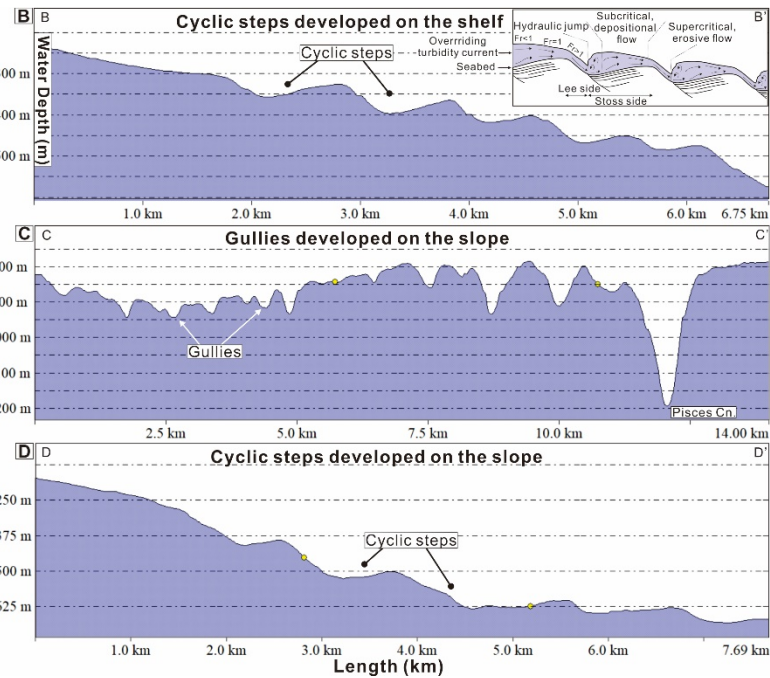
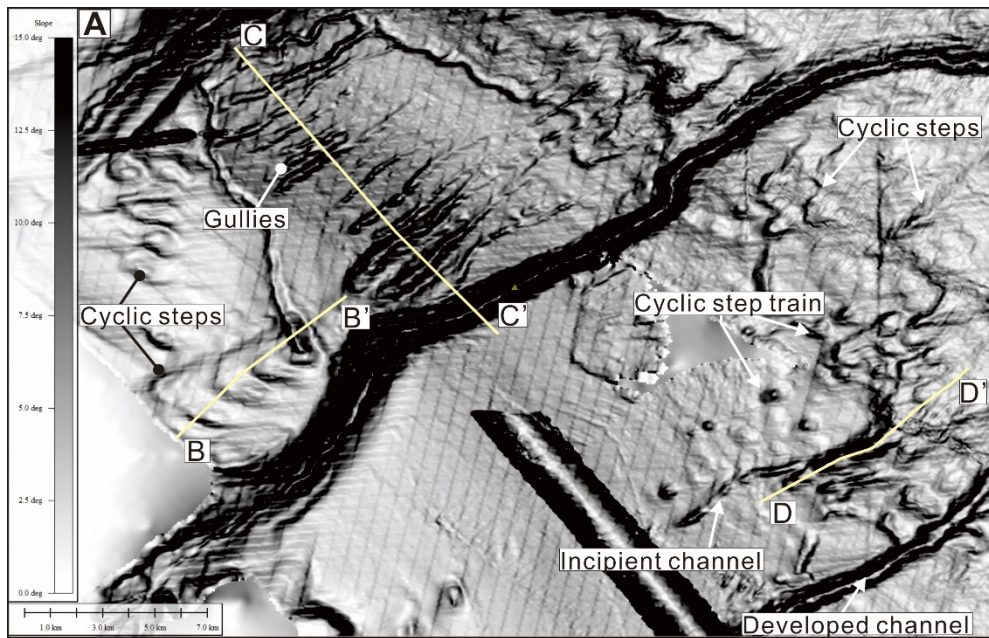


Figure 9

